SAND2012-2814C

Solute Distribution and Mechanical Properties of Ultra-Fine-Grained Al-Mg Alloys (SAND2012-2814 C)

Richard A. Karnesky[1], Nancy Y. C. Yang[1], Chris San Marchi[1], Troy D. Topping[2], Zhiui Zhang[2], Ying Li[2], Enrique J. Lavernia[2]

[1]Sandia National Laboratories, 7011 East Ave, Livermore, CA, 94550, USA
[2]University of California, Davis, 1 Shields Ave, Davis, CA, 95616, USA

Keywords: atom-probe tomography, cryomilled, magnesium, nanocrystalline

Abstract

Ultra-fine-grained (d~200 nm) Al-Mg alloys exhibit outstanding strength due to both Hall-Petch grain-size strengthening and solid-solution strengthening. When the solubility limit is exceeded, some Mg segregates to grain boundaries. This impacts both thermal stability and mechanical properties. In this study, alloys with between 0 wt.% Mg (pure Al) and 10.5 wt.% Mg are made by ball milling powders in liquid nitrogen, and consolidated by hot isostatic pressing and extrusion. The alloys are exposed to temperatures up to 500 deg. C. Microhardness and tensile behavior are measured and correlated with the microstructure, as measured by local-electrode atom-probe tomography, X-ray diffraction, and electron microscopy.

Introduction

Ultra-fine-grained Al-Mg (UFG Al-Mg) alloys exhibit a high specific strength, while retaining good ductility [1-6]. This strength comes from a combination of Hall-Petch strengthening due to the small grain size (d~200 nm) and from Mg that is in solid solution in the alloy. The latter is limited by how much Mg can stay in solution. While the solid solubility of Mg in α-Al at the eutectic temperature (450 ºC) is very high (16 at.%), the solubility at room temperature is only about 1% [7]. When the solubility limit is exceeded, alloys will be driven to produce Mg-rich β-phase, Al_3Mg_2, which nucleate and grow from GP zones with intermediate phases [8]:

$$\alpha\text{-Al} \rightarrow \beta'' \rightarrow \beta' \rightarrow \beta \quad (1)$$

These phases often segregate to grain boundaries, which will also often have elemental Mg segregation. This has a deleterious effect on mechanical properties and corrosion resistance. While this decomposition process has been shown on supersaturated samples aged for years at ambient temperature [8], supersaturated alloys are used with between about 3-7% Mg (exceeding the solid solubility limits between 200-300 ºC). Furthermore, alloys with a very fine grain size have been shown to be able to have greatly super-saturated solutions [9]. While there has been some promise that bulk UFG Al-Mg, prepared by consolidating nanocrystalline powders, may share in this enhanced solubility and do display excellent mechanical properties [1-4], these materials undergo a number of thermal processing steps and may be exposed to elevated temperatures in use. The temporal evolution of the materials during these treatments has not been reported. In this paper, we show how the grain size and distribution of Mg in UFG Al-Mg changes with processing and aging.

Experimental Methods

Spray-atomized Al alloy powders were cryogenically milled in liquid nitrogen, vacuum degassed at 400-450 °C in order to remove water vapor, the process control agent, and other residual volatile contaminants [10-11], consolidated by hot isostatic pressing, and extruded into 33 mm diameter rods to form UFG Al-Mg with between 0 wt.% Mg (pure Al) and 10.5 wt.% Mg. In

order to test the thermal stability, samples were aged in air at 300 or 500 for as long as 16 days. Specimens were prepared after each processing step to analyze grain size and chemistry.

In order to measure the grain size, x-ray diffraction measurements were made of both powder and consolidated samples. The latter were ground to a 1 μm surface finish. The Scherrer approximation using the (111) peak from XRD spectra has been shown to be provide an estimate of the crystallite size consistent with the grain size determined by TEM for similar alloys [12], and so was employed for these measurements.

Specimens for atom-probe tomography were prepared from powder in a method similar to one described in Ref. [13]. An FEI Helios NanoLab dual-beam scanning electron microscope/focused ion beam with an Omniprobe manipulator was used to prepare tips from cryomilled UFG Al-7 Mg (wt.%) powder that had been thermally degassed. A small particle was welded to the Omniprobe with Pt deposition and the particle was mounted to a post on an Imago microtip array. Selecting an individual particle is quicker and involves less FIB damage than methods that involve cutting a post from a particle [14-16]. Pt welds were made on two opposite sides of the particle. Gallium ions accelerated to 28-280 pA were used to cut holes that were filled in with Pt to make the mortise and tenon joints, and to annularly mill the powder into a sharpened tip. During the final stage of milling, the ion beam was reduced to 5 keV and 47 pA to minimize Ga implantation [14]. Atom-probe specimens were prepared from bulk consolidations by mechanically grinding material to a square cross-section of ca. 200x200 μm^2 and electropolishing the tips in 10 vol.% perchorlic acid in actic acid, followed by polishing in 2 vol.% perchloric acid in butoxyethanol.

The tips were analyzed on a Cameca (formerly Imago) local-electrode atom-probe (LEAP) tomograph operated with 200 kHz voltage pulsing with a 15% pulse fraction at 60 K. Lower temperatures runs on other tips led to premature tip fracture. Data were analyzed with Imago's computer program IVAS.

The Vickers microhardnesses of the six microalloys were measured using a 100 g weight for 3 s dwell time at ambient temperature on samples ground to a 1 μm surface finish. Ten measurements were recorded on each sample.

Results

Changes During Processing

The grain size of UFG Al-7.5 Mg was measured as a function of processing step and is presented in Table I. It has previously been speculated that the majority of grain growth during the processing stages occurs during the degassing step [10]. The powders are generally exposed to the highest temperature for the longest time during degassing. After cryomilling, for example, nanocrystalline powders are degassed at a temperature near 400 °C for up to a day in order to remove water vapor, the process control agent, and other residual volatile contaminants [10-11]. In this set of experiments degassing increased the grain size by a factor of 4, whereas consolidation increased the grain size by a factor of less than 2, indicating that grain growth occurs primarily during degassing.

Table I. Grain size in Al-7.5 Mg, as function of processing step

Condition	Grain Size (nm)
Atomized	80
Atomized, degassed	280
Adomized, cryomilled	30
Adomized, cryomilled, degassed	140
Adomized, cryomilled, degassed, HIPed, extruded	220

Due both to the fine grain size (30 nm) and the small amount of segregation (possibly because of the nonequilibrium nature of cryomilled powders), there is no immediately obvious segregation in cryomilled Al-7.5Mg powders. Some segregation may be present, as can be seen in the compositional profile in Figure 1a. This composition profile was generated by taking a moving average over 100 atoms in a prism that had a 2 x 2 nm^2 square cross section, as has been used in nanocrystalline Ni-W alloys with grain sizes between 3-20 nm. As in those alloys, the Mg composition in the Al-7.5Mg powder fluctuates about a mean value of 3 ± 1 at%, with larger deviations from this mean value occurring at periodic intervals approximately equivalent to the grain size (~30 nm). The magnitude of this enrichment is on the order of 7 at%. Mg segregation becomes more apparent after thermal exposure associated with degassing. This segregation can be depicted in isoconcentration surfaces from LEAP tomographic datasets, such as in Figure 1b for cryomilled and degassed Al-7.5Mg powder. Parts of multiple grains are visible with nominally 140 nm diameter grain size; these boundaries are highlighted by Mg segregation. The composition between different powder particles may be inhomogeneous, but the composition measured within grains is similar across multiple datasets, and is only 25% of the nominal composition of the alloy. The Mg available for solid solution strengthening at ambient temperatures is thus not significantly higher than the amount of Mg in coarse-grained 5000-series alloys before β-phase Al_3Mg_2 precipitation is observed. The excess Mg may lower grain boundary energy and can form MgO at boundaries. These features can slow grain growth and movement at elevated temperatures.

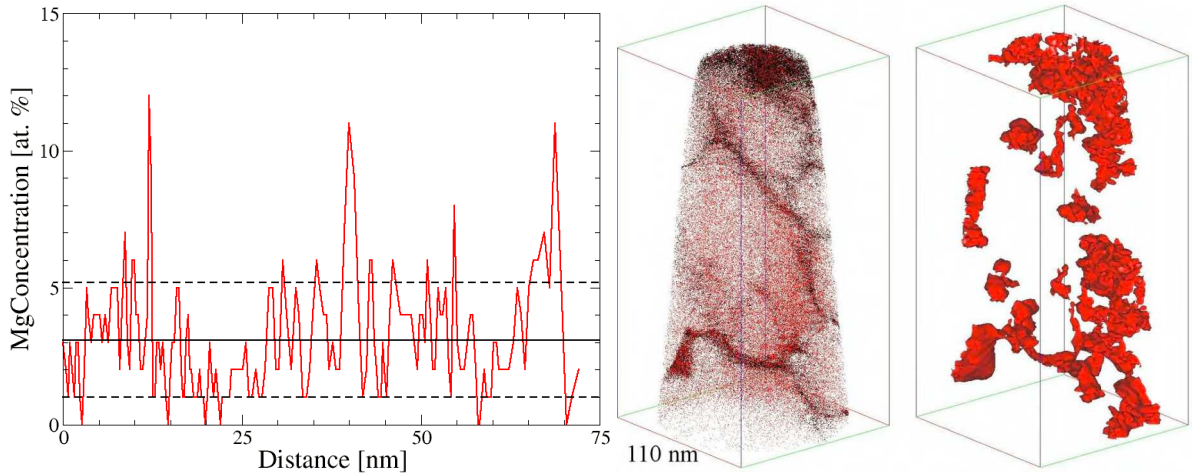

Figure 1. (a) Mg composition profile for cryomilled Al-7.5Mg powder from LEAP tomographic data. The black solid and dashed horizontal lines correspond to the mean and standard deviation of the alloy composition. Three Mg peaks are separated by approximate size of the grains in the cryomilled powder (30 nm). (b) Mg (red) and Ga (black) atoms in a LEAP tomographic reconstruction of degassed cryomilled 5083Al powder and a 5.5 at% Mg isoconcentration surface showing Mg segregation to grain boundaries.

Thermal Stability of UFG Al-Mg

The thermal stability of UFG Al-Mg on aging in air at 300 °C and 500 °C is shown in Figure 2.

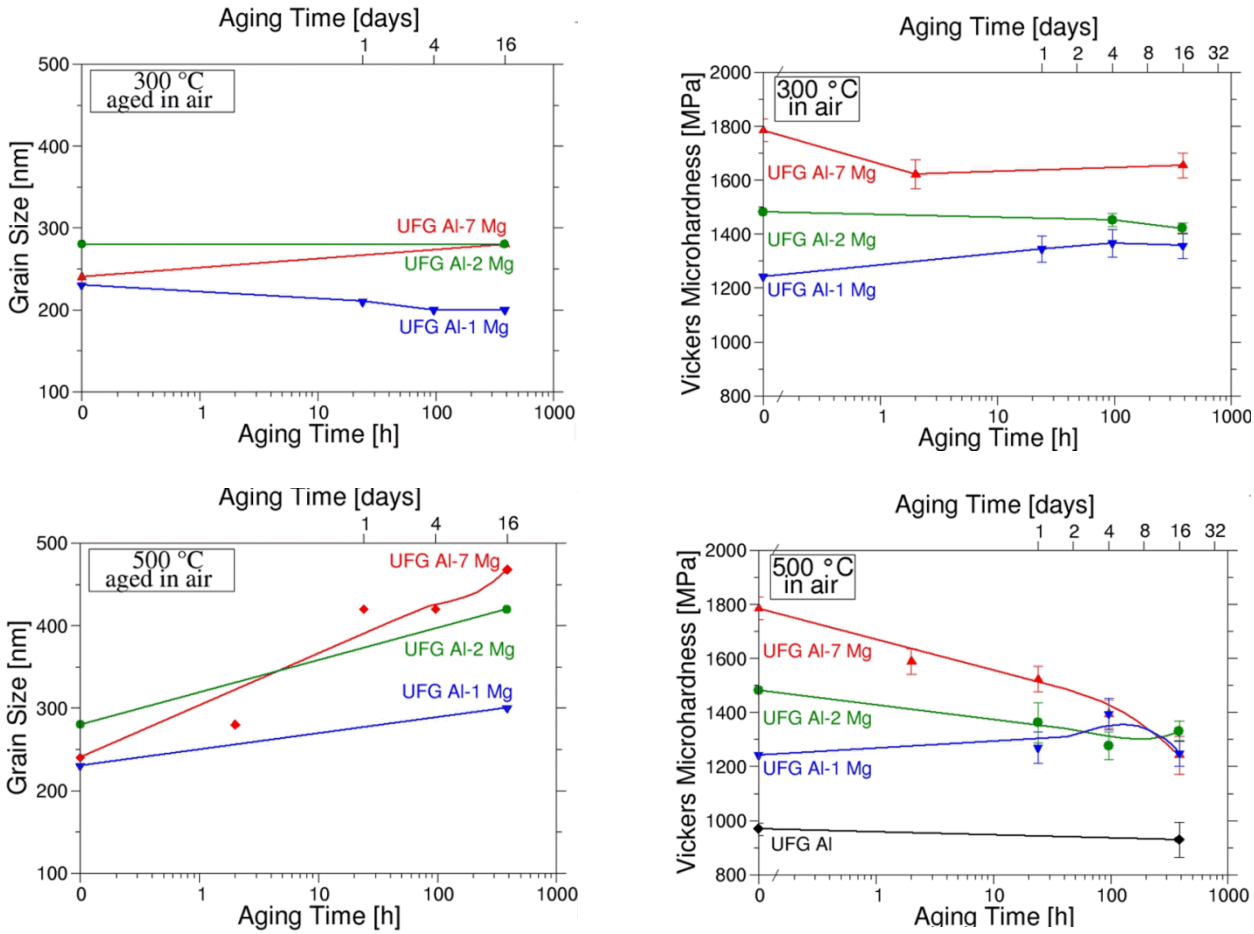

Figure 2. The grain size and microhardness of UFG Al-Mg is stable at 300 °C for 16 days. At 500 °C, there is considerable grain growth, resulting in a concomitant decrease in microhardness.

Discussion

The diffusivity of Mg in Al is relatively large at the typical degassing temperature of 400 °C (D = 9.44 x 10-15 m2/s and is probably larger at grain boundaries). Estimated diffusion distances for Mg in Al at 400 °C are on the order of the powder size (tens of microns) after just a few hours. High mobility of Mg may facilitate grain growth, in addition to Mg segregation. Moreover, high diffusivity of Mg may aid formation of MgO when sufficient oxygen is present, which may retard grain growth.

The UFG Al-Mg-based alloys in this study exhibit high strength at ambient temperature. This is expected to arise from the fine grain size, solid-solution strengthening (particularly by Mg), and a high dislocation density. MgO and solute segregation at grain boundaries may stabilize grain structure through Zener pinning and by lowering the free energy of the mostly high-angle boundaries when the material is annealed at high temperatures. Very little precipitation is observed, so precipitate strengthening via the Orowan mechanism or precipitate shear is not thought to be significant.

The grain size component of strengthening is described by the Hall-Petch relationship:

$$\sigma_{HP} = \frac{k}{\sqrt{d}}; \qquad (2)$$

where k is the locking parameter (k~0.2 MPa m$^{0.5}$) and d is the grain size (230<d<450 nm for the alloys in this study). The grain size exceeds the nanocrystalline grain sizes that are typically associated with the so-called "inverse Hall-Petch" effect (where grain sizes smaller than do not obtain as high of a strength as predicted by Eq. 1 and those smaller than ca. 10 nm lead to weakening. Equation 2 yields $300 < \sigma_{HP} < 420$ MPa for these alloys. This mechanism can explain a majority of the strength exhibited by the alloys.

Mg solid solution strengthening accounts for the remaining 50-150 MPa of strength in the alloys. The superposition of strengthening mechanisms is shown in Figure 4.

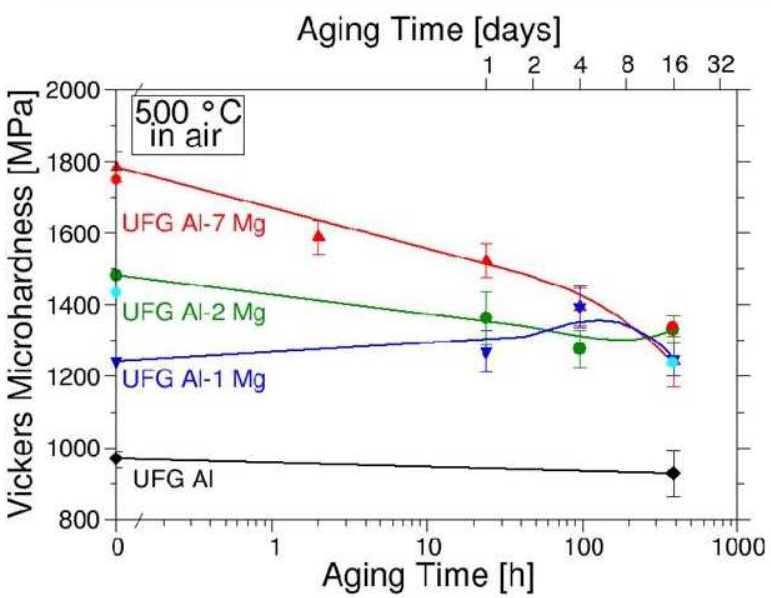

Figure 4. Vickers Microhardness of samples aged at 500 C in air. Symbols with no uncertainty bars are the calculated expected microhardness from summing the grain size strengthening expected based on XRD measurements of grain size and solid solution strengthening expected based on LEAP tomographic measurements of Mg concentration. They are in good agreement with the measured values.

Acknowledgements

The authors wish to thank Northwestern University and especially D. Isheim for focused-ion beam preparation of some atom-probe specimens. We would also like to thank our colleagues (too numerous to name) at SNL/CA and UC Davis for their assistance and support of this work.

Sandia National Laboratories is a multi-program laboratory managed and operated by Sandia Corporation, a wholly owned subsidiary of Lockheed Martin Corporation, for the U.S. Department of Energy's National Nuclear Security Administration under contract DE-AC04-94AL85000.

References

1. B.Q. Han, E.J. Lavernia, and F.A. Mohammed, "Tension and Compression of Bulk Al-7.5 wt% Mg Alloy," *Phil. Mag. Lett.,* 83 (2003), 89-96.

2. D. Witkin et al., "Al-Mg Alloy Engineered with Bimodal Grain Size for High Strength and Increased Ductility," *Scripta Mater.,* 49 (2003), 297-302.

3. G.J. Fan et al., "Deformation Behavior of an Ultrafine-Grained Al-Mg Alloy at Different Strain Rates," *Scripta Mater.,* 52 (2005), 929-933.

4. Z. Lee et al., "Bimodal Microstructure and Deformation of Cryomilled Bulk Nanocrystalline Al-7.5Mg Alloy," *Mater. Sci. Eng. A,* 410-411 (2005), 462-467.

5. K.M. Youssef et al., "Nanocrystalline Al-Mg Alloy with Ultrahigh Strength and Good Ductility," *Scripta Mater.*, 54 (2006), 251-256.

6. R. Kapoor et al., "Influence of Fraction of High Angle Boundaries on the Mechanical Behavior of an Ultrafine Grained Al-Mg Alloy," *Mater. Sci. Eng. A*, 527 (2010), 5246-5254.

7. Kent R. Van Horn, ed., Aluminum, vol. 1 (Metals Park, OH: American Society for Metals, 1967), 362-375.

8. M.J. Starink and A.-M. Zahra, "Low-Temperature Decomposition of Al-Mg Alloys: Guinier-Preston Zones and L12 Ordered Precipitates," *Phil. Mag. A*, 76 (1997), 701-714.

9. A. Calka, W. Kaczmarek, and J.S. Williams, "Extended Solid Solubility in Ball-Milled Al-Mg Alloys," *J. Mater. Sci.*, 28 (1993), 15-18.

10. D.B. Witkin and E. J. Lavernia, "Synthesis and Mechanical Behabior of Nanostructured Materials via Cryomilling," *Prog. Mater. Sci.*, 51 (2006), 1-60.

11. B. Ahn et al., "Effect of Degassing Temperature on the Microstructure of Nanocrystalline Al-Mg Alloy," *Mater. Sci. Eng. A*, 463 (2007), 61-66.

12. Z. Zhang, F. Zhou, and E.J. Lavernia, "On the Analysis of Grain Size in Bulk Nanocrystalline Materials via X-Ray Diffraction," *Met. Mater. Trans. A*, 34 (2003), 1349-1355.

13. M.K. Miller and K.F. Russell, "Atom Probe Specimen Preparation with a Dual Beam SEM/FIB Miller," *Ultramicroscopy*, 107 (2007), 761-766

14. K. Thompson et al., "In Situ Site-Specific Preparation for Atom Probe Tomography," *Ultramicroscopy,* 107 (2007), 131-139.

15. P. Cho, et al., "Application of Focusted Ion Beam to Atom Probe Tomography Specimen Preparation from Mechanically Alloyed Powders," *Microsc. Microanal.*, 13 (2007), 347-353.

16. D. Saxey, et al., "Atom Probe Specimen Fabrication Methods Using a Dual FIB/SEM," *Ultramicroscopy*, 107 (2007), 756-760.